Magnetic Barkhausen noise from strain-induced martensite during low cycle fatigue of 304L austenitic stainless steel

Alain Vincent, Ludovic Pasco, Michel Morin, xavier Kleber, M. Delnondedieu

Magnetic Barkhausen noise from strain-induced martensite during low cycle fatigue of 304L austenitic stainless steel

A. Vincent [a,*], L. Pasco [a], M. Morin [a], X. Kleber [a], M. Delnondedieu [b]

[a] *Groupe d'Etudes de Metallurgie Physique et de Physique des Matériaux-UMR CNRS 5510, Institut National des Sciences Appliquées, 69621 Villeurbanne Cedex, France*

[b] *EDF, Site des Renardieres, 77818 Moret sur Loing Cedex, France*

The magnetic Barkhausen noise from strain induced α'-martensite is investigated during low cycle fatigue (LCF) of 304L steel. The influence of cold-rolling prior to fatigue is also examined. Both cold rolling and LCF induce α'-martensite that is characterised by a high field Barkhausen peak, clearly distinguishable from the δ ferrite peak. For the same volume fraction of α'-martensite, the Barkhausen activity is more intense for martensite induced by cold-rolling than for martensite induced by LCF. For LCF, the intensity of the peak varies tremendously along a $\sigma = f(\varepsilon)$ loop, being enhanced in the tension part of the loop and strongly decreased in the compression part. Neither the applied stress nor the plastic strain controls the Barkhausen activity alone. A composite model is used to estimate the variation of the internal stress of type II within the martensite phase. It is concluded that the Barkhausen activity is controlled by this internal stress.

Keywords: Fatigue; Austenitic stainless steel; Martensite; Magnetic Barkhausen emission; Non-destructive testing

1. Introduction

The evaluation of the residual life of materials submitted to cyclic loading is of great practical importance. This requires non-destructive tools that enable one to assess changes in the material state since the beginning of service. Generally, fatigue of materials is characterised by successive stages: (i) microstructure changes and accumulation of crystalline defects due to the irreversibility of cyclic deformation mechanisms; (ii) micro-crack nucleation and growth; (iii) development of a critical crack (from the fast growth of one crack or by coalescence of several micro-cracks) leading to rupture. For several austenitic steels widely used in the chemical industry and in power plant construction, stage (i) includes formation of martensite, which plays a significant role in material behaviour [1–3] and damage mechanisms [4,5]. Hence, non-destructive characterisation of strain-induced martensite could provide a valuable contribution to assessing the residual life. For that purpose the magnetic properties of the material can be used to characterise strain-induced α'-martensite in the non-magnetic γ matrix [6–9]. However, another possible way would consist of measuring the magnetic Barkhausen noise (MBN) induced by the dynamic reorganisation of the magnetic microstructure of martensite during cyclic magnetisation of the material. This method is well known to provide information more closely related to the microstructure than macroscopic magnetic measurements. Furthermore, its applicability to studying strain-induced α'-martensite in austenitic steel subjected to tensile strains has been demonstrated recently [10].

The aim of this work is to investigate and understand the relationship between the magnetic Barkhausen emission and the material changes during

* Corresponding author. Tel.: +33 472438257; fax: +33 472438539.
E-mail address: alain.vincent@insa-lyon.fr (A. Vincent).

low-cycle fatigue (LCF). In fact, it is well known that generally MBN is sensitive not only to the properties of the magnetic phase but also to its stress state (stress being of internal or applied origin) [11–13]. Moreover, internal stresses are expected to be induced by the martensitic transformation itself, or by the further inhomogeneous plastic deformation of the composite-like material (martensite grains embedded in the austenite matrix). Therefore, it is expected that, in such processes, Barkhausen noise can be influenced by these internal stresses. In order to investigate these phenomena, a device has been developed to allow in situ MBN measurements in a push–pull machine, including measurements under load.

In this paper, first the experimental conditions, including material preparation, fatigue conditions and in situ MBN apparatus, are described. In the second part, the results concerning MBN features obtained throughout the fatigue life and their variation along a fatigue loop are presented. In the last part, the observed results are discussed in terms of both the magnetic phases present in the austenitic matrix and the internal stresses of type II which are induced by plastic deformation of inhomogeneous materials.

2. Experimental details

2.1. Materials

A 304L austenitic stainless steel was investigated, with the following composition (in wt.%): 0.029 C, 0.37 Si, 1.86 Mn, 0.029 P, 18.0 Cr, 10.0 Ni, 0.04 Mo. The material was solution annealed at 1120 °C followed by water quenching. The average austenite grain size was 75 μm. Twins were present in the grains. The initial volume fraction of ferritic phases (mainly δ ferrite, as shown by metallographic observations) was measured by neutron diffraction (ND). It was found very low: 0.3 vol.%. Several steel plates were cold rolled prior to the fatigue test, in order to investigate the influence of a prestrain on the material behaviour. For these specimens the initial volume fraction of ferritic phases measured by ND was 2.6 vol.%.

The specimens were carefully machined and polished. For in situ MBN measurements, they had a dumbbell shape with a diameter of 10 mm and a useful length of 20 mm, their axis being parallel to the rolling direction. A few flat specimens with a rectangular cross section of 8×6 mm^2 (useful length 16 mm) were also prepared, for the purpose of observing surface damage.

2.2. Fatigue tests

The specimens were fixed to the push–pull machine (INSTRON 3555) by means of screwed heads. Symmetrical push–pull fatigue tests were conducted in air at room temperature. The tests were performed under total strain control with a constant strain rate of 4×10^{-3} s^{-1}. A clip-on extensometer was used to measure and control the strain. To perform a MBN measurement, the fatigue test could be interrupted at any current point of the fatigue stress–strain loop. Then, the applied stress was controlled to be constant while performing the MBN measurement. It should be mentioned that some micro-creep occurs during this constant stress stage. However, the creep strain remained small with respect to the plastic strain involved throughout one fatigue loop and it has been verified that globally these cycling interruptions did not significantly change the fatigue behaviour of the material (strain hardening, fatigue life). Finally, the cyclic loading was resumed, continuing along the stress–strain loop to the next point of measurement.

2.3. Magnetic Barkhausen noise measurements

The apparatus for measuring MBN during LCF tests is presented in Fig. 1. The excitation magnetic circuit, including a pair of two U-shaped cores made of a high permeability iron–nickel alloy, was closed through the grips of the fatigue machine and the specimen. The U-shaped cores were hinged. Thus, during the fatigue test the grips were left moving freely, i.e., without any contact with the U-shaped cores. On the contrary, the U-shaped cores were connected to the cylindrical grips during MBN measurements. Two coils wound around these U-shaped cores were supplied by a current with a

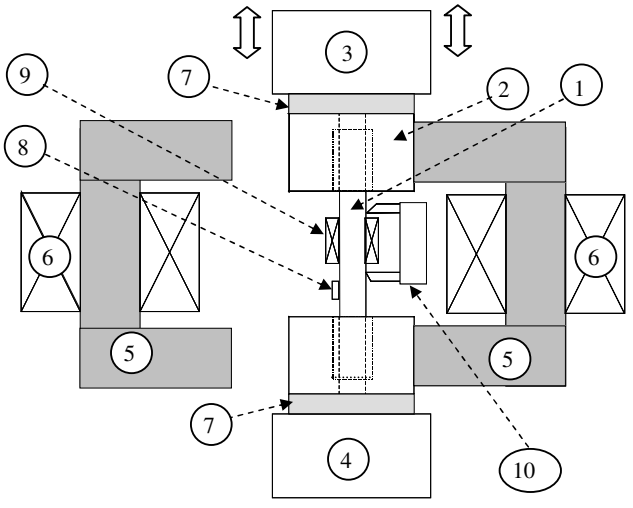

Fig. 1. Schematic of the experimental arrangement used for MBN measurements in the push–pull fatigue machine: 1, specimen; 2, screwed steel grip; 3, machine loader; 4, load cell; 5, double U-shape electromagnets (left arm open = fatigue configuration; right arm closed = MBN measurements configuration); 6, magnetising coils; 7, magnetic insulation; 8, Hall probe; 9, MBN encircling coil; 10, clip-on extensometer.

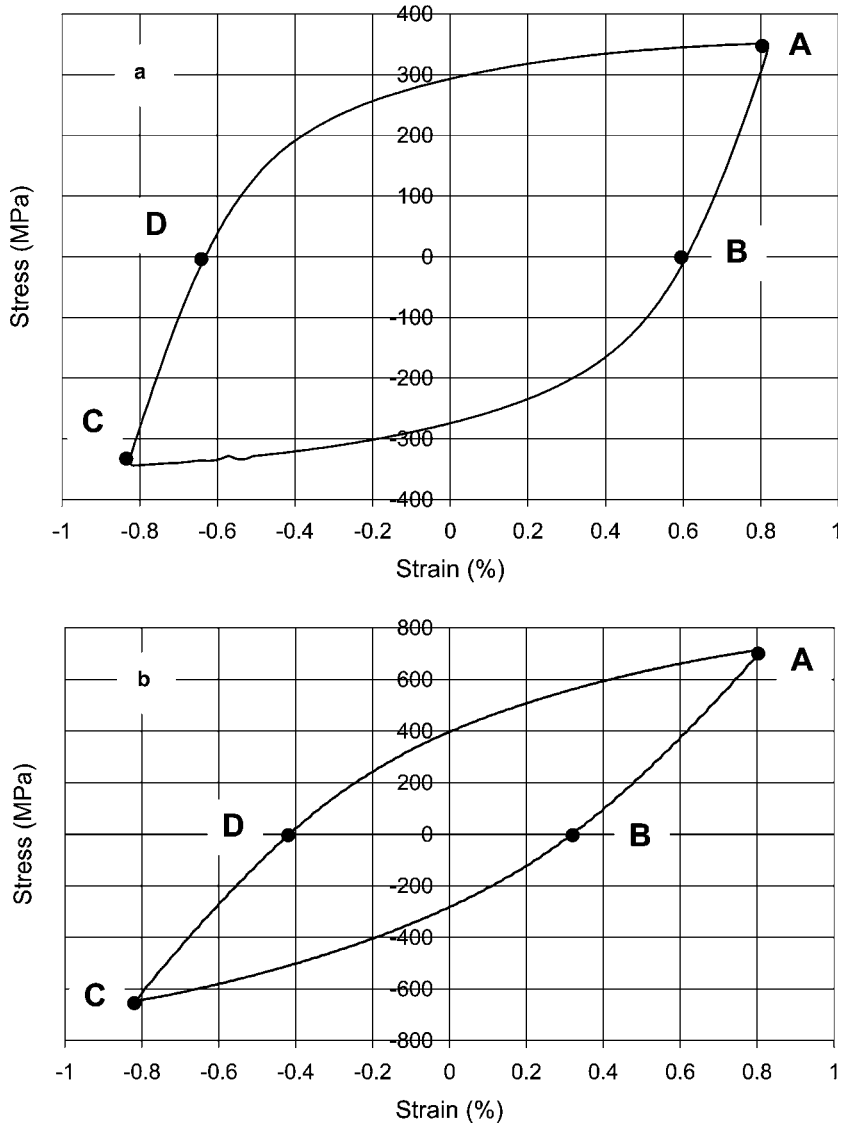

Fig. 2. Stabilised stress–strain loop for 304L specimens cycled at $\varepsilon_a = \pm 0.8\%$: (a) as received, cycle number $N = 16$; (b) cold worked, cycle number $N = 16$.

triangular waveform. The samples were magnetised from saturation to saturation. The frequency of magnetisation was 0.4 Hz, which is low enough to avoid the generation of eddy currents in the material. The magnetic field, H, induced in the specimen was measured at its surface by a Hall sensor. The MBN signals were detected using a surrounding coil probe located in the useful part of the specimen. Following a pre-amplification stage, MBN was selected from the overall signal through a 2-kHz high pass filter. Then, the instant[1] root mean square (RMS) value of the noise voltage, hereafter noted V_{RMS}, was delivered. The details of the electronic device can be found in previous papers [14,15]. In this work, the MBN response is always peak shaped and is characterised by simple parameters: the area under the peak,[2] A_{RMS}, which characterises the overall Barkhausen noise activity, and the magnetic field at the maximum of V_{RMS}, H_M, which gives the peak position. Since the recorded peaks were most often of small amplitude, it has been checked that the signals were actually due to MBN emitted by the 304L material and not by the surroundings (grips, U-shaped cores, etc.). For that purpose, a specimen made of aluminium was tested under the same operating conditions: as expected no peak was observed. For the 304L steel, MBN measurements were achieved regularly throughout the life of the material at the four particular points of the stress–strain loops shown in Fig. 2: the two extremities of the loop and the two points where the applied stress is nil.

[1] The integration time of the RMS circuit was fixed to 25 ms for every measurements.

[2] For calculating A_{RMS}, the background noise V_N is subtracted from the total noise V_{RMS} according to $V_M = \sqrt{V_{RMS}^2 - V_N^2}$.

Furthermore, for a few selected cycles, the MBN response was measured throughout a complete loop.

3. Results

3.1. Mechanical behaviour and damage

The steel was tested at room temperature for two strain amplitudes $\varepsilon_a = \pm 0.4\%$ and $\pm 0.8\%$. The material behaviour during a stabilised loop is illustrated in Fig. 2(a) and (b) for the material fatigued at $\varepsilon_a = \pm 0.8\%$. For the cyclic hardening curves (maximum and mean stress of each cycle, denoted σ_{max} and σ_{mean} in Fig. 3, respectively) the as received material exhibits a short stage of strain hardening followed by a weak softening stage, and finally a weak secondary hardening stage up to rupture (Fig. 3). In contrast, the cold-rolled material exhibits only a softening stage (Fig. 3). Furthermore, it should be noted that the stress–strain $\sigma = f(\varepsilon)$ loops are non-symmetrical for the cold-rolled material, with a higher maximal stress in tension (see Figs. 2 and 3). The behaviour tends to become more symmetrical with increasing cycle number.

Note that for the specimens cycled at $\varepsilon_a = \pm 0.4\%$, the behaviours are globally similar, while diverging only on the following minor points: (i) the softening stage is more marked and the secondary hardening does not appear for the as received material; (ii) the softening is less marked for the prestrained specimen, and accordingly, the $\sigma = f(\varepsilon)$ loops keep their asymmetrical character throughout the life; (iii) the cycle number to rupture, hereafter noted N_R, amounts to 10^4 and 1.4×10^4 cycles for the as received and cold-rolled materials, respectively.

In order to follow the possible influence of damage on MBN results, the appearance and growth of cracks has been observed by optical microscopy on specific specimens with flat surfaces. Up to about $0.5N_R$, only a few short cracks (size < 100 μm) were observed for all conditions (see example in Fig. 4). Beyond $0.5N_R$ the density of surface cracks increased more rapidly. Once a macrocrack was formed, a decrease in σ_{max} could be observed on the stress hardening curve (see Fig. 3) followed rapidly by rupture. Although the paper is not focused on damage mechanisms, it is worth mentioning that, as is usually reported for such stainless steels [1], many short cracks were of the transgranular type (most often parallel to the slip bands), while only few were of the intergranular type.

3.2. Microstructural changes along the fatigue life

Depending on temperature, material composition, and loading amplitude, LCF may induce various micro-

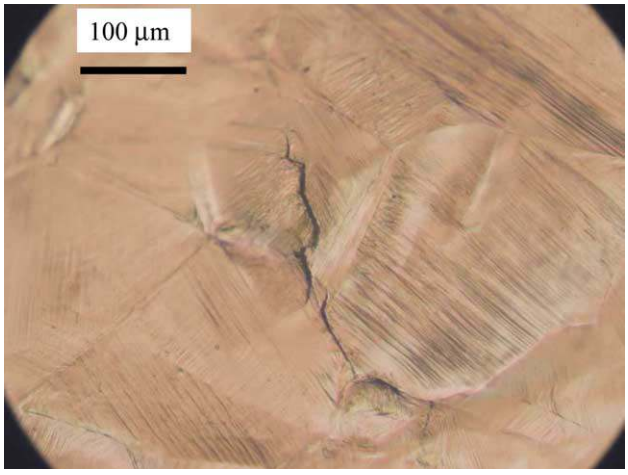

Fig. 4. Optical micrograph showing surface microcracks: as received material; $\varepsilon_a = \pm 0.8\%$; $N/N_R = 0.5$.

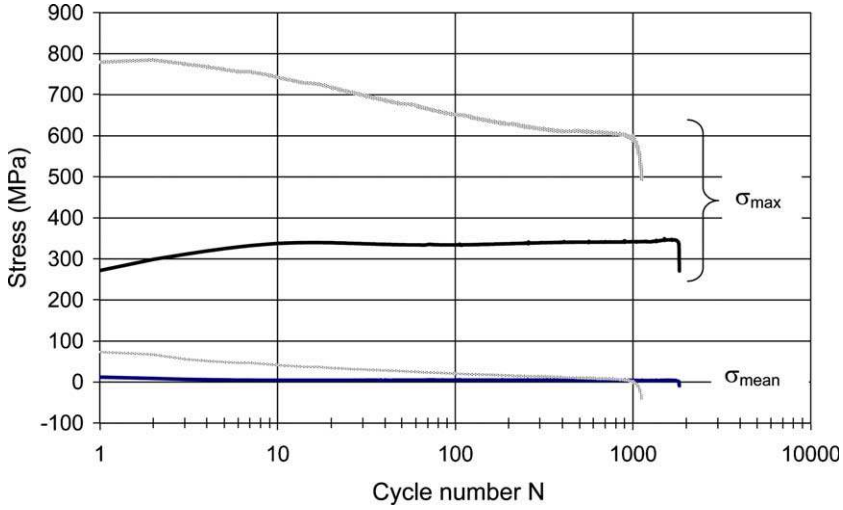

Fig. 3. Cyclic hardening/softening curves (σ_{max} and σ_{mean}) for 304L specimens cycled at $\varepsilon_a = \pm 0.8\%$ for as received (dark lines) and cold worked (grey lines) materials.

structural changes in metastable austenitic steels, including phase transformation of the austenite into ε and α'-martensite, dislocation multiplication and formation of dislocation cells, and micro twinning. For the purpose of analysing the MBN results on the 304L steel, we have been focused on the appearance of α'-martensite (even if ε-martensite was formed, since it is not magnetic it would not contribute to MBN). The variation of the α'-martensite content induced by cycling has been measured in selected fatigued states either by neutron diffraction (ND) or X ray diffraction (XRD). For the as received material, the increase of α'-martensite induced by LCF was hardly detectable following fatigue both at $\varepsilon_a = \pm 0.4\%$ and $\varepsilon_a = \pm 0.8\%$. For the cold-rolled material the increase was 1.5 and 2.5 vol.% after 60% of the fatigue life at $\varepsilon_a = \pm 0.4\%$ and at $\varepsilon_a = \pm 0.8\%$, respectively.

3.3. Typical variations of the MBN fingerprint along the fatigue life

First, the $V_{RMS} = f(H)$ fingerprints before fatigue cycling are shown in Fig. 5. For the as received material, it can be seen that, despite the large amplification of the voltage scale, the fingerprint is almost flat (Fig. 5(a)). In contrast, for the cold-rolled material, the $V_{RMS} = f(H)$ response exhibits a well developed peak (Fig. 5(b)).

For fatigued specimens, as will be seen in the next section, it is more attractive to study the MBN at point A of the $\sigma = f(\varepsilon)$ loops, where the MBN activity is the largest for a given cycle. Then, Figs. 6 and 7 show typical MBN fingerprints corresponding to different numbers of cycle for the as received specimens fatigued at $\varepsilon_a = \pm 0.4\%$ and $\pm 0.8\%$. For $\varepsilon_a = \pm 0.4\%$ (Fig. 6), a small peak can be seen from the first quarter of the first cycle, while MBN activity was not evident for the non-loaded conditions (Fig. 5(a)). It should be noticed that this peak is centred in the low field range ($H_M < 1$ kA/m). The peak height varies only slightly with an increase in the number of fatigue cycles. At $\varepsilon_a = \pm 0.8\%$, the same peak, with a greater height, is also observed for the first quarter of the first cycle (Fig. 7(a)). Then, it is striking that a second peak, centred around $H_M \cong 5$ kA/m, appears after few additional cycles. Furthermore, this peak grows with an increase in the number of cycles (Fig. 7(b) and (c)). In fact, as shown in Fig. 8, the MBN activity A_{RMS} does increase regularly during the first part of the material life, but it seems to decrease during the last part of the life leading to rupture. It

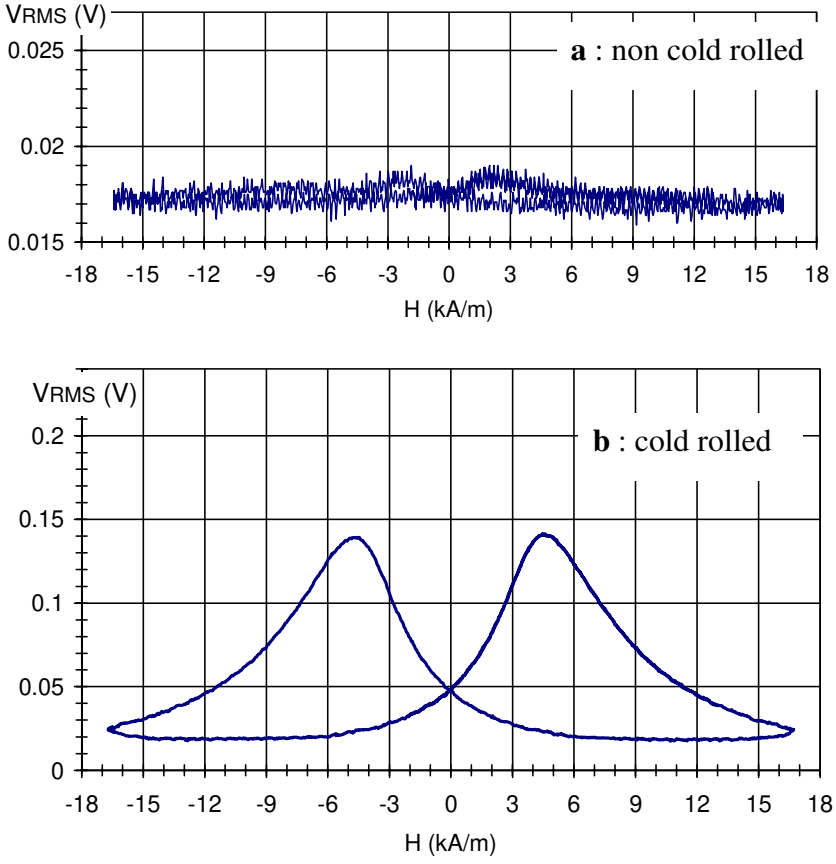

Fig. 5. Barkhausen RMS response $V_{RMS} = f(H)$ before fatigue: (a) as received 304L steel; (b) cold rolled 304L steel. Note the great difference in the V_{RMS} scale between a and b.

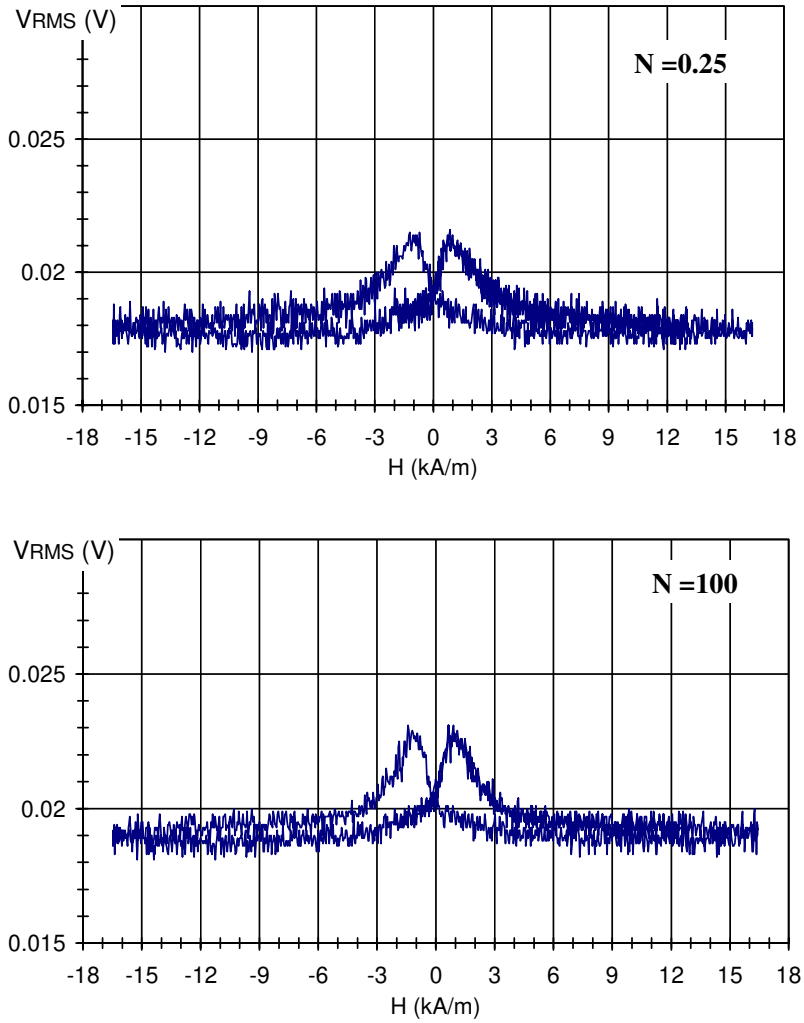

Fig. 6. Selected Barkhausen RMS responses $V_{RMS} = f(H)$ measured at $\sigma = \sigma_{max}$ for the as received 304L steel cycled at $\varepsilon_a = \pm 0.4\%$; $N = 0.25$ (a quarter of the first cycle) and $N = 100$.

should be noticed that this stage roughly corresponds to the development of surface cracks.

For the cold rolled 304L material, loading and fatigue did not modify the single peak shape of the initial response shown in Fig. 5. As a matter of fact, the first loading up to σ_{max} increased the peak height of about 30% and 50% for the cycling at $\varepsilon_a = \pm 0.4\%$ and $\varepsilon_a = \pm 0.8\%$, respectively. Then, with further cycling, Fig. 9 shows that the MBN activity A_{RMS} does not change markedly for the material fatigued at $\varepsilon_a = \pm 0.4\%$, while it increases continuously for the material fatigued at $\varepsilon_a = \pm 0.8\%$. These trends seem to be weakly modified for the last measurements before rupture, i.e., in the range where macrocracks grow and hence probably interfere with the magnetic measurements.

3.4. MBN measurements along a stabilised cycle

First, Fig. 10 shows the quite different $V_{RMS} = f(H)$ fingerprints that are observed for the four particular points A, B, C, D of a stabilised stress–strain loop (example of the 600th cycle of a cold rolled specimen fatigued at $\varepsilon_a = \pm 0.8\%$). Indeed, the MBN activity appears to be strongly influenced by the position of the measuring point, being enhanced by a tensile stress and reduced by a compressive one. The fact that a marked difference also appears between the two measurements at $\sigma = 0$ (points B and D of the hysteresis loop – Fig. 2) is more striking. This means that the applied stress is not the only parameter that governs the MBN activity, i.e., the plastic strain history also plays a significant role. The same features are observed for all testing conditions. As a matter of fact, the MBN activity is weaker for the as received specimens, but a similar difference between the two points of measurement at $\sigma = 0$ is also observed: for the 100th cycle and $\varepsilon_a = \pm 0.8\%$, the MBN activity is $A_{RMS} = 0.134$ V kA/m and $A_{RMS} = 0.081$ V kA/m for the high field peak measured at points B and D, respectively.

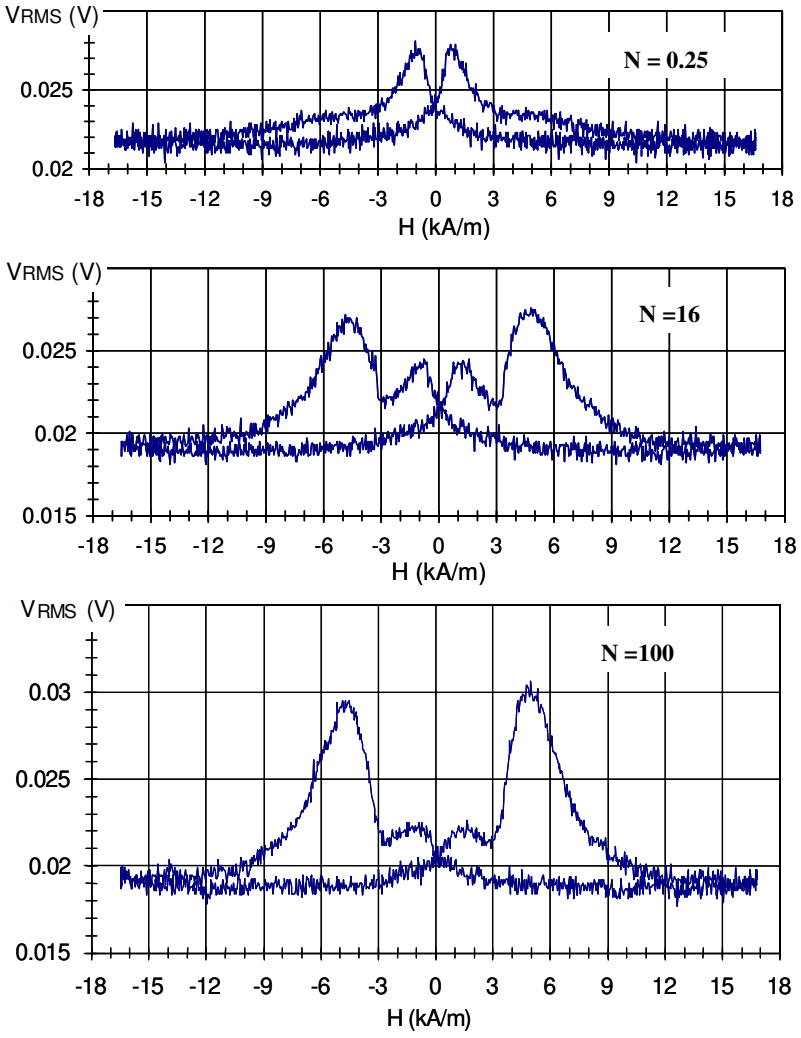

Fig. 7. Selected Barkhausen RMS responses $V_{RMS} = f(H)$ measured at $\sigma = \sigma_{max}$ for the as received 304L steel cycled at $\varepsilon_a = \pm 0.8\%$; $N = 0.25$, $N = 16$ and $N = 100$.

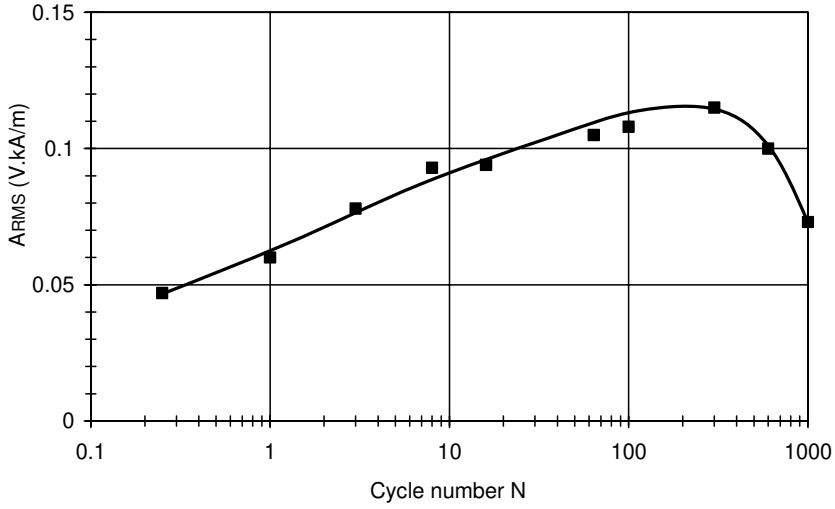

Fig. 8. Variation of the Barkhausen noise activity A_{RMS} (high field peak) measured at point A shown in Fig. 2 ($\sigma = \sigma_{max}$) vs. N for the as received 304L steel fatigued at $\varepsilon_a = \pm 0.8\%$.

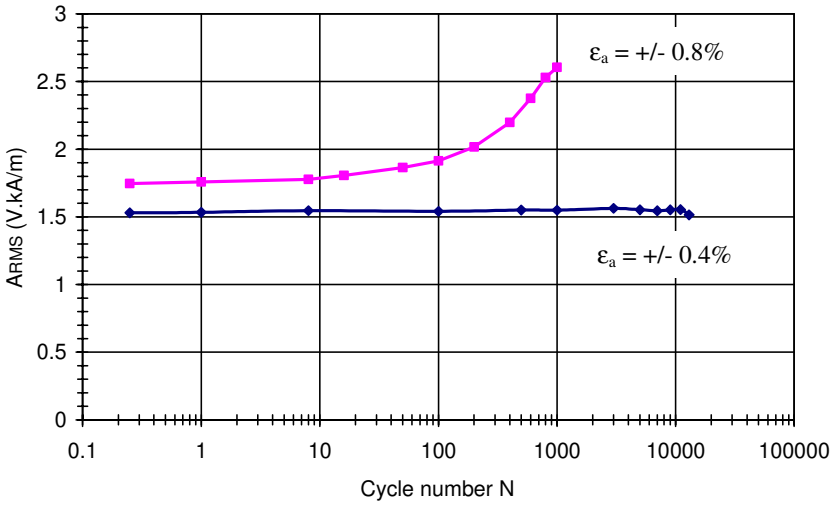

Fig. 9. Variation of the Barkhausen noise activity A_{RMS}, measured at point A shown in Fig. 2 ($\sigma = \sigma_{max}$), vs. N for the cold-worked 304L steel.

Figs. 11 and 12 show the variations of the quantity A_{RMS} throughout a complete cycle (600th cycle for the same specimen as in Fig. 10). Plotted either as a function of stress or as a function of plastic strain, A_{RMS} variations exhibit a hysteresis behaviour, which confirms that the MBN activity is not a simple function of a single macroscopic parameter.

4. Discussion

In Section 4.1, all the MBN data are discussed from a qualitative point of view, then, in Section 4.2, variations of MBN activity along a fatigue loop are analysed quantitatively.

4.1. General analysis of MBN in 304L steel

The origin and features of MBN activity in ferromagnetic materials have been reported in many papers. However, for all the results presented in Section 3, it should be mentioned that the MBN activity is only linked with a very low volume fraction of ferromagnetic phase (few vol.% as attested by XRD or ND). As a matter of fact, two types of ferritic phases are included in the XRD or ND data: (i) the δ ferrite is inherent to the elaboration process and hence it is present in the as received state; (ii) the α'-martensite is induced by monotonic or cyclic straining of the material. Since the δ ferrite content is not expected to vary during the loading of the material, all the variations of the volume fraction of ferritic phase can be ascribed to the strain induced α'-martensite.

For the as received material, at the end of the first quarter of the first cycle at $\varepsilon_a = \pm 0.4\%$, a small peak was seen in the MBN response (Fig. 6: $N = 0.25$), which was hardly visible prior to fatigue (Fig. 5(a)). This peak cannot be ascribed to α'-martensite because at this stage of fatigue the plastic deformation is so small ($\cong 0.3\%$) that martensite is not expected to be strain induced. Moreover, the low field position of the peak ($H_M \cong 1$ kA/m) does not correspond at all to the position generally observed for the α'-martensite (2.5–3 kA/m [14]). It should be mentioned that the peak position may be affected by the presence of internal demagnetizing fields as the ferromagnetic phases are arranged in small islands embedded in a non-magnetic matrix. However, since the possible influence of these demagnetizing fields is expected to lead to an increase in H_M, this confirms that only the δ ferrite can be responsible for the observed peak. The difference between the peak height observed prior to loading and under load is due to the well known effect of a tensile stress applied parallel to the magnetisation axis that enhances the MBN activity in iron based materials [11]. Attributing this peak to ferrite δ is also consistent with the fact that the peak height varies only weakly with the cycle number, as the vol.% of the δ ferrite is likely to remain constant during LCF. Hence, the weak variation of the peak height can be associated to the variations of σ_{max} and the plastic deformation of the δ ferrite during LCF.

Furthermore, this interpretation remains sound when the behaviour of the same material fatigued at $\varepsilon_a = \pm 0.8\%$ is considered. First, at the end of the first quarter of the first cycle (Fig. 7: $N = 0.25$), the same peak as that observed at $\varepsilon_a = \pm 0.4\%$ appears, but it is higher than the previous one. This is not surprising, the value of σ_{max} is greater there than for $\varepsilon_a = \pm 0.4\%$. Second, in contrast to the material fatigued at $\varepsilon_a = \pm 0.4\%$, the new peak that appears when the number of cycles is increased (Fig. 7: $N = 16$–100) can be ascribed to the strain induced α'-martensite: (i) it grows vs. cycle number as the α'-volume fraction is expected to do; (ii) its position ($H_M \cong 4$–5 kA/m) is consistent with the

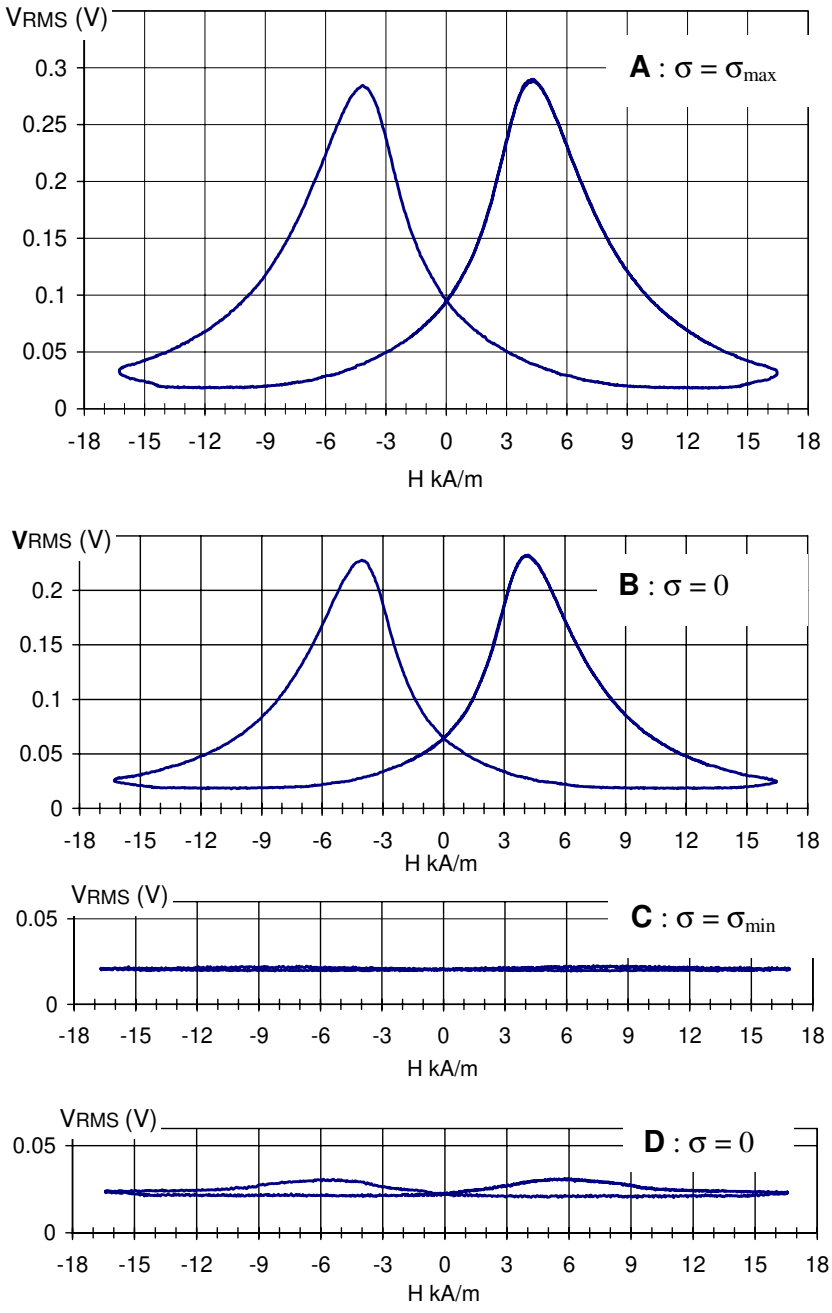

Fig. 10. Selected Barkhausen RMS responses $V_{RMS} = f(H)$ measured at points A, B, C and D of a stabilised $\sigma = f(\varepsilon)$ loop ($N = 600$) for a cold rolled 304L steel cycled at $\varepsilon_a = \pm 0.8\%$.

field range where martensite MBN peaks are observed in fully martensitic steels.

Concerning the cold-rolled 304L, first it is noted that the field position of the peak induced by cold rolling before fatigue (Fig. 5(b)) is the same as that of the α' peak induced by fatigue in the as received material (Fig. 7: $N = 16$–100). Since, in addition, ND results have shown a significant increase in the α'-martensite volume fraction induced by cold rolling, this peak can also be ascribed to strain induced martensite without any reluctance, which is also consistent with the work reported by O'Sullivan et al. [10]. As shown in Fig. 9 the A_{RMS} activity does not vary significantly with further cycling at $\varepsilon_a = \pm 0.4\%$, while a 40% increase is observed at $\varepsilon_a = \pm 0.8\%$, which is, from a qualitative point of view, in agreement with the larger increase of α'-martensite in the material cycled at $\pm 0.8\%$ than in the material cycled at $\pm 0.4\%$.

However, from a quantitative point of view, it should be noted that the intensity of MBN emitted by the α'-martensite induced by cold rolling and that induced by LCF are not exactly of the same order. Indeed, from the results obtained for the cold-rolled material cycled at $\varepsilon_a = \pm 0.4\%$, it can be seen that for about the same

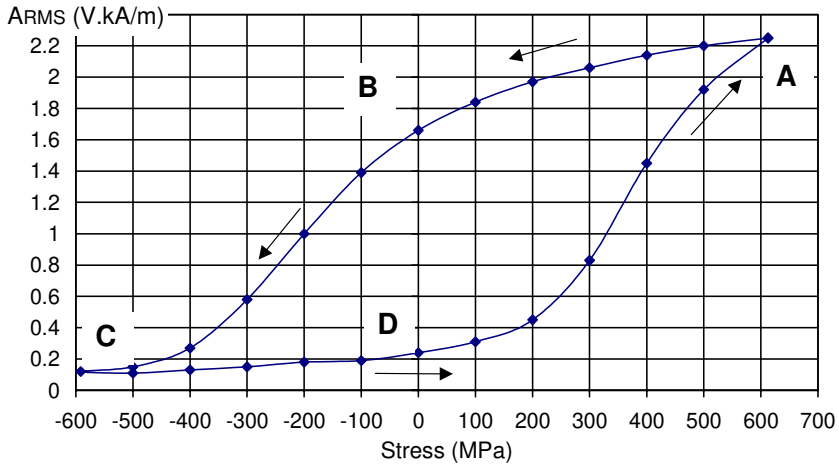

Fig. 11. Variation of $A_{RMS} = f(\sigma)$ along a complete stress–strain loop: cold rolled 304L steel; $\varepsilon_a = \pm 0.8\%$; $N = 600$.

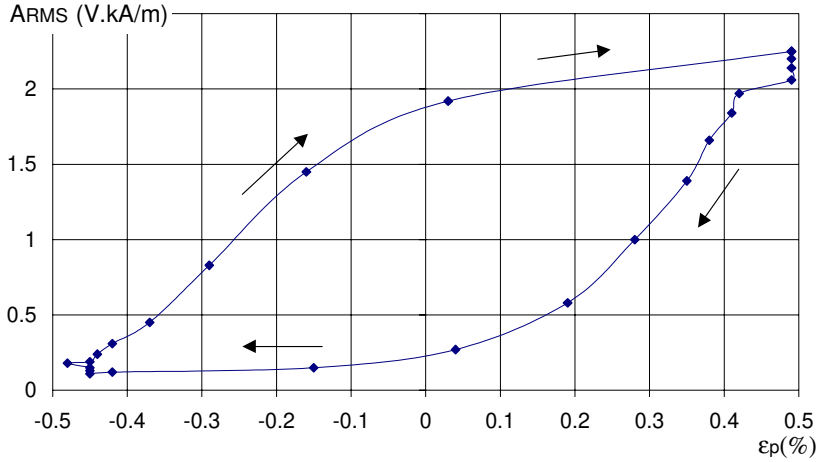

Fig. 12. Variation of $A_{RMS} = f(\varepsilon_p)$ along a complete stress–strain loop: cold rolled 304L steel; $\varepsilon_a = \pm 0.8\%$; $N = 600$.

increase in the α' volume fraction (i.e., 2% by cold-rolling and 1.5% by fatigue, measured under the same conditions), the increase in MBN activity seems to be much lower for LCF induced than for cold-rolled induced α'-martensite. This can not be easily explained, in terms of microstructure, since it has been reported by many authors that mechanisms of creation and microstructural features of strain induced martensite are very similar for both modes of loading. However, an explanation for this surprising behaviour will be derived at the end of the following section.

Finally, the most problematic feature of the present results is the influence of the position of measurement along a single fatigue loop: this is analysed quantitatively in the following section.

4.2. A model for the variation of MBN activity throughout a fatigue loop

First of all, it should be pointed out that, to our knowledge, the reversal of the transformation $\gamma \rightarrow \alpha'$ during room temperature loading has not been reported in the literature for our alloy. Then, the volume fraction of α'-martensite can only increase monotonically by very small increments from cycle to cycle. For instance, for the greatest increase in α'-martensite volume fraction induced by fatigue, i.e. 2.5%, the mean increase per cycle is 2.5×10^{-5}. Therefore, the volume fraction of α'-martensite can be considered as quasi constant along a single fatigue loop. Hence, such a parameter cannot open a way for explaining the huge variations of A_{RMS} along such a loop. Then, the MBN variations can only be due to variations of the physical and mechanical properties of martensite, as suggested by many works carried out on fully ferritic steels that have shown the marked influences of stress and plastic deformation on the MBN response of these materials [11–15]. It should also be noted that a strong influence of these mechanical parameters has been reported for the macroscopic magnetic properties of austenitic steels [6]. As a matter of fact, the plastic deformation state of α' units created during the previous fatigue cycles is not expected to vary

along the current fatigue loop either. Indeed, due to the high value of yield stress usually attributed to martensite [3], it is likely that it behaves elastically during further LCF. Furthermore, Fig. 11 has shown that the applied stress is not a suitable parameter for describing A_{RMS} variations. Therefore, the internal stress in the martensite phase should be taken into account rather than the macroscopic applied stress. Indeed, the 304L steel is a composite-like material, the previously created martensite grains playing the role of hard particles embedded in the soft austenite phase. Hence, high level internal stresses are expected to be induced in the α' phase.

In order to estimate the stress variation within the martensite grains, the "equivalent homogeneous inclusion" method can be used. This means that martensite grains are considered as inclusions embedded in a continuous matrix of austenite, i.e., the polycrystalline character of austenite is not taken into account. Then, for a composite material, a general expression of the mean internal stress tensor in the inclusion has been developed by Withers et al. [16]. In fact, in the present case, the calculation can be simplified from the following argument. As mentioned previously the behaviours of austenite and martensite mainly differ by their yield stress rather than by their elastic constants. Hence, during the elasto-plastic loading the mismatch strain between inclusion and matrix is mainly of plastic origin. Then, in Withers et al.'s model both stiffness tensors of inclusion and matrix can be taken as equal to that of the homogenised material, hereafter noted $\boldsymbol{C}$. This leads to the expression for the total stress within the inclusion:

$$\boldsymbol{\sigma_I} + \boldsymbol{\sigma} = (1-f)\boldsymbol{C}(\boldsymbol{S}-\boldsymbol{I})\boldsymbol{\varepsilon}^{T} + \boldsymbol{\sigma}, \tag{1}$$

where is $\boldsymbol{\sigma}$ the applied stress, f is the volume fraction of inclusions, $\boldsymbol{S}$ is the Eshelby's tensor, $\boldsymbol{I}$ is the identity matrix and $\boldsymbol{\varepsilon}^{T}$ is the transformation strain tensor.

As proposed by Withers et al., $\boldsymbol{\varepsilon}^{T}$ is deduced from the argument that, if the plastic strain $\boldsymbol{\varepsilon}_P$ in the matrix is assumed to be uniform, the stress field in the composite is identical to that of an elastic matrix containing inclusions strained in a stress free manner by $-\boldsymbol{\varepsilon}_P$, so that for a uniaxial loading:

$$\boldsymbol{\varepsilon}^{T} = -\boldsymbol{\varepsilon}_P = -\frac{\varepsilon_P}{(1-f)}[1,-1/2,-1/2,0,0,0], \tag{2}$$

where ε_P is the axial macroscopic plastic strain of the overall material.

In this form, the model can be applied once the aspect ratio and the orientation of the ellipsoidal inclusion are defined. It has been reported that strain induced α'-martensite appears as blocky and lenticular [2]. In fact, the shape and orientation are distributed, but these distributions are not known. Therefore, in applying the model to describe the stress variation in α'-martensite during a fatigue loop, we consider a spherical shape for inclusions, which is expected to roughly represent the mean effect of shape and orientation distributions. Furthermore, it should be emphasised that at the beginning of the current loop, the initial internal stress in α'-martensite is not known: this should result from cold-work, as suggested by the asymmetry of the $\sigma = f(\varepsilon)$ loop and/or from the $\gamma \rightarrow \alpha'$ transformation itself. Therefore, only the variation of the total stress within martensite, $\Delta\boldsymbol{\sigma}_{\alpha'}$, can be calculated, which from Eqs. (1) and (2) is finally expressed:

$$\Delta\boldsymbol{\sigma}_{\alpha'} = \boldsymbol{C}(\boldsymbol{S}-\boldsymbol{I})\boldsymbol{\varepsilon}_P[-1,+1/2,+1/2,0,0,0] + \boldsymbol{\sigma} \tag{3}$$

In order to test the validity of the model and the inherent assumptions, it is useful to verify that the relationship between the variations of the stress component parallel to the axis of magnetisation (hereafter noted $\Delta\sigma_{\alpha'H}$) and the intensity of MBN is similar to that obtained for fully martensitic steels. Thus, A_{RMS} has been plotted vs. $\Delta\sigma_{\alpha'H}$ in Fig. 13 for various loading conditions. For the as received specimen, only the four specific points A, B, C, D, are available since the number of measurements was limited due to the low intensity of MBN (Fig. 13(a)). In contrast, for the cold-rolled specimens a number of data are available throughout a complete loop (Fig. 13(b) and (c)). Anyway, all these plots show clearly that the MBN activity and the variation of stress within martensite exhibit a bijective relation. This very well supports the assumption that the internal stress within martensite is the parameter controlling the MBN activity. Furthermore, for the specimen subjected to large enough stress variations, it should be noted that the A_{RMS} vs. $\Delta\sigma_{\alpha'H}$ curve is sigmoid shaped, which is very similar to that exhibited by fully martensitic steels subjected to tension–compression uniaxial loading [17]. As mentioned by Blaow et al. [17], such a smooth shape is presumably linked to the fact that the $V_{RMS} = f(H)$ response of α'-martensite remains one-peak shaped both under tension and compression loading. In contrast, for other steel microstructures such as equiaxial ferrite or ferrite + cementite, the response changes from one-peak to multiple-peak shape from tension to compression loading [11,15,17], thus producing less continuous variation of A_{RMS} vs. stress. Concerning the physics of the MBN, these remarks argue in favour of a single type of domain walls in martensitic structures to be responsible for the MBN. As suggested by the results of Saquet et al. [14] these should be 180° domain walls since martensitic structures do not produce acoustic Barkhausen noise.

Finally, still concerning the A_{RMS} vs. stress relationship, it should be noted that it is not unique for the different conditions reported in Fig. 13. This is partly due to the different volume fractions of α'-martensite corresponding to each set of experimental conditions. Indeed, if one tries to normalise the A_{RMS} variations by the α' volume fraction, one still get non-coinciding curves. As a matter of fact, it is likely that the residual stress of type

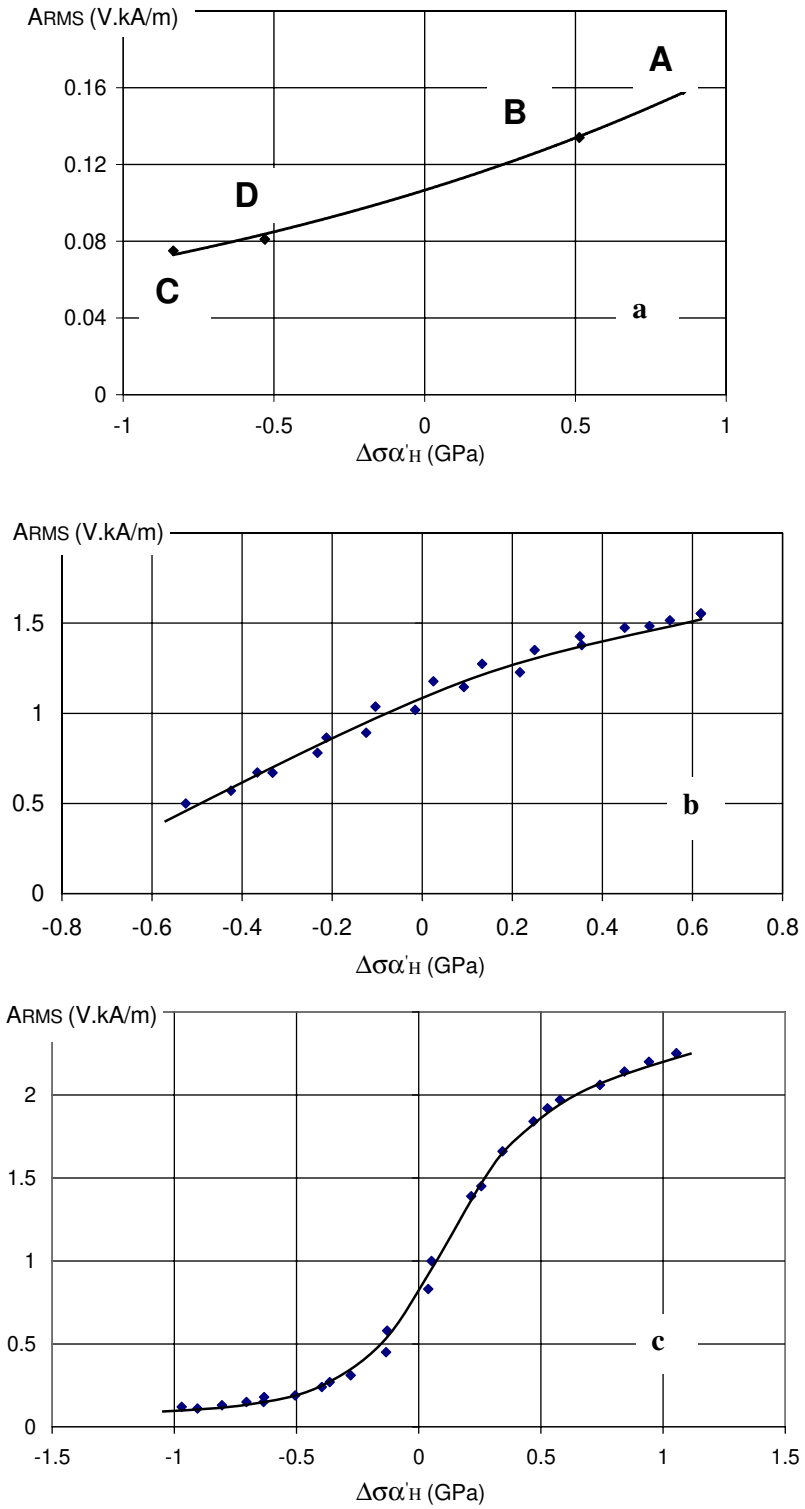

Fig. 13. A_{RMS} vs. internal stress (within α'-martensite) change along a stress–strain loop: (a) as received, $\varepsilon_a = \pm 0.8\%$, $N = 100$; (b) cold rolled, $\varepsilon_a = \pm 0.4\%$, $N = 5000$; (c) cold rolled, $\varepsilon_a = \pm 0.8\%$, $N = 600$.

II present at the beginning of the current loop shifts each range of $\Delta\sigma_{\alpha' H}$ variations with respect to the origin of stress. This residual stress could result from the volume increase linked to the $\gamma \rightarrow \alpha'$ transformation, on the one hand, and from the plastic strain mismatch between γ and α' phases during cold-work, on the other hand. Thus, the α'-martensite for the three conditions reported in Fig. 13 should be affected by different residual stres-

ses: of compression type for the material of Fig. 13(a) (non-cold-worked), and of tension type for the material of Fig. 13(b) and (c) (cold-worked). The latter stresses are more markedly relaxed by LCF preceding the measured cycle, as attested to by the more important decrease of the asymmetry of the $\sigma = f(\varepsilon)$ loop for the material tested at $\varepsilon_a = \pm 0.8\%$ (see Fig. 3(b)). Unfortunately, it is not yet possible to make a quantitative correction for such a difference, these residual stresses being not available. However, it can be noticed that the curvature of the A_{RMS} vs. stress relationship is positive and negative in Fig. 13(a) and (b), respectively. Owing to the sigmoid shape exhibited in Fig. 13(c) that is obtained for the largest stress variation, this suggests that the aforementioned curve shift would be negative for conditions of Fig. 13(a) and positive for Fig. 13(b). This corresponds to negative and positive residual stresses, respectively, as argued above.

Finally, it should be mentioned that this strong sensitivity of MBN to stresses is also presumably responsible for some surprising behaviours noted in Section 3. On the one hand, the residual stress of tension type in the cold-worked material could explain the surprisingly high level of MBN activity in this material regarding the low volume fraction of martensite. On the other hand, the surprising decrease of A_{RMS} vs. N in the last part of the life of the as received material might also be linked with a decrease of the stress within the α'-martensite in this stage, presumably due to some stress relaxation near surface cracks. However, it is not clear why this phenomenon is less marked in the cold-worked material.

5. Conclusion

The effect of strain induced α'-martensite on MBN characteristics has been investigated in 304L steel subjected to LCF under various conditions. This work shows that despite the very low volume fractions of ferromagnetic phases present in such steels the MBN technique is quite suitable for characterising the variations of the martensite content induced by LCF.

In particular, the appearance of α'-martensite vs. number of cycles was observed in the as received material, the characteristics of the α' peak being clearly distinguished from those of the δ ferrite peak. Furthermore, these MBN results show that α'-martensite is created early in the life of the as received material. This confirms that the beginning of creation of α'-martensite (induced by LCF) is not correlated to the appearance of secondary hardening.

The most important feature of the MBN due to α'-martensite is its great sensitivity to the position of measurement along the fatigue loop. These variations can be described on the basis of a composite-like behaviour of the material. From the proposed model the calculated stress within the α'-martensite phase appears as the parameter controlling the variation of the MBN activity along the fatigue loop.

The intensity of MBN due to α'-martensite induced by cold rolling seems to be more important than that of α'-martensite induced by LCF. This is likely to be due to the large residual stress of type II that are of tension type in α'-martensite induced by cold rolling.

Owing to this high sensitivity to stress, it appears that coupling the MBN technique with another NDT technique able to determine the martensite volume fraction would provide a convenient means to characterise the residual stress within martensite. However, for further application on real components it would be necessary to investigate the influence of the multiaxiality of the loading conditions to which such components are subjected.

Acknowledgements

The work is supported by the EU through a cost shared Project (FIS5-1999-00280) that is gratefully acknowledged.

M. Niffenenger is gratefully acknowledged for achieving the measurements of the martensite content by ND.

References

[1] Baudry G, Pineau A. Mater Sci Eng 1977;28:229.
[2] Bayerlein M, Christ H-J, Mughrabi H. Mater Sci Eng A 1989;114:L11.
[3] Altenberger I, Scholtes B, Martin U, Oettel H. Mater Sci Eng A 1999;264:1.
[4] Mei Z, Morris JW. Metall Trans A 1990;21:3137.
[5] Baffie N, Stolarz J, Magnin T. Matériaux Tech 2000;5–6:57.
[6] de Backer F, Schoss V, Maussner G. Nucl Eng Des 2001;206(2–3): 201.
[7] Hecker SS, Stout MG, Staudhammer KP, Smith JL. Metall Trans A 1982;13:619.
[8] Kaleta J, Zietek G. Fatigue Fract Eng Mater Struct 1998;21:955.
[9] Lang M, Johnson J, Schreiber J, Dobmann G, Bassler HJ, Eifler D, et al. Nucl Eng Des 2000;198:185.
[10] O'Sullivan D, Cotterell M, Meszaros I. NDT & E Int 2004;37(4):265.
[11] Gathelier-Rothea C, Chicois J, Fougeres R, Fleischmann P. Acta Mater 1998;46(14):4873.
[12] Anglada-Riviera J, Padovese LR, Capo-Sanchez J. J Magn Magn Mater 2001;231:299.
[13] Chicois J, Tapuleasa D. Cofrend congress on non destructive testing, 22–26th September 1997, Nantes, France. Cofrend Press. p. 607–13
[14] Saquet O, Chicois J, Vincent A. Mater Sci Eng A 1999;269:73.
[15] Kleber X, Vincent A. NDT & E Int 2004;37:439.
[16] Withers P, Stobbs WM, Pedersen OB. Acta Metall 1989;37(11):3061.
[17] Blaow M, Evans JT, Shaw BA. Acta Mater 2005;53:279.